On the 40 GHz Remote versus Local Photonic Generation for DML-based C-RAN Optical Fronthaul

Luis Vallejo, *Member, IEEE,* Jose Mora, Dong-Nhat Nguyen, Jan Bohata, Vicenç Almenar, Stanislav Zvanovec, *Senior Member, IEEE,* Beatriz Ortega, *Member, IEEE*

***Abstract*—Local and remote photonic millimeter wave (mmW) signal generation schemes are theoretically and experimentally evaluated in order to compare both approaches for practical deployment in a cloud-radio access network (C-RAN) fronthaul network. The paper presents a full comprehensive formulation of the frequency response of a system based on a directly modulated laser transmitting data over 40 GHz signal generated by external carrier suppressed modulation and optical frequency multiplication. Theoretical and experimental characterization of the system response at baseband and mmW band for local and remote generation setups show very good agreement. The remote configuration leads to higher electrical output power (i.e. 15 dB higherin 25 km fiber links) due to the combined effect of chirp and fiber dispersion than the local generation setup in the mmW band, although intermodulation distortion is higher in the former case. Transmission experiments using quadrature phase-shift keying (QPSK) signal with 250 MHz bandwidth centered at 0.5 GHz over 10 and 25 km fiber links also confirm the superior performance of the remote setup, whereas the local setup leads to similar results to optical back-to-back (OB2B) measurements, which is also validated with data signal centered at different frequencies within the laser bandwidth frequency range. Finally, experimental results show the quality of the recovered signals in terms of error vector magnitude (EVM) as a function of the received electrical power and demonstrate that no further penalties are introduced by photonic mmW signal generation with respect to electrical back-to-back (EB2B) levels.**

***Index Terms*—Cloud radio access networks, millimeter wave, optical access networks.**

I. Introduction

THE continuous growth of the number of smartphones, wearables, tablets or internet of things devices, and the emerging of new multimedia services, such as cloud access, 4K/8K high definition video, augmented virtual reality, online gaming or social networking exceed the capabilities of the current mobile network. As expected [1], there will be 5.3 billion total internet users (66% of the global population) by 2023, the number of mobile devices will increase up to 13.1 billion in 2023 and 1.4 billion of these will be 5G. Moreover, an unprecedented number of people had to change their workplace from office to home during the Covid-19 pandemic in 2020 [2], which means a further substantial increase of the applications, such as voice calls, video conferences or entertainment and messaging applications and a total growth of mobile data traffic between 10 and 20% during lockdown periods. The evolution of the legacy mobile communication networks up to 5G and beyond will enable downlink experience user over 1Gb/s, 30 bps/Hz spectral efficiency, latency lower than 1 ms, connection density of 1,000,000 device/km^2 and high efficient power consumption [3].

Due to the congestion of lower microwave bands employed in conventional cellular services, millimeter wave (mmW) band has been proposed for 5G mobile communications with large spectral availability and delivered throughput. Therefore, mmW new radio (NR) is the new interface for mobile users in 5G [4, 5, 6]. From the network perspective, existing optical fibers and also free space optics (FSO) links provide fixed/mobile convergence with sufficient bandwidth to deliver high-speed services over long distances with low cost, high reliability and low latency [7].

Photonic generation of mmW signals offers low phase noise and frequency tunability in addition to the use of electronics components with reduced bandwidth. Although different approaches based on dual-mode sources [8], mode-locked lasers [9, 10], pulsed lasers [11] or nonlinear optical effects [12, 13, 14] amongst others have been previously demonstrated, external lithium niobate Mach-Zehnder modulators (MZM) can be considered as the most popular approach due to easy implementation, high quality and efficient mmW signal generation. Depending on the bias point of the modulator, optical single sideband (SSB), double sideband (DSB) and also carrier suppression (CS) techniques [15] can be employed to provide frequency multiplying with a factor from 2 up to 12 [12, 16].

Although the CAPEX and OPEX reduction is a benefit in cloud-radio access network (C-RAN) networks, the availability and costs of the optical infrastructure become critical especially in the small-cell environment [17].

Fig. 1 illustrates the variety of access segments forming the global telecommunication network which includes indoor mmW small cells access as well as fiber broadband access in residential areas and also outdoor emerging small-cell C-RAN systems. As depicted in Fig. 1, the C-RAN architecture hosts the baseband units (BBUs) at the central office (CO) separated from the remote radio heads (RRH). This is enabled by the

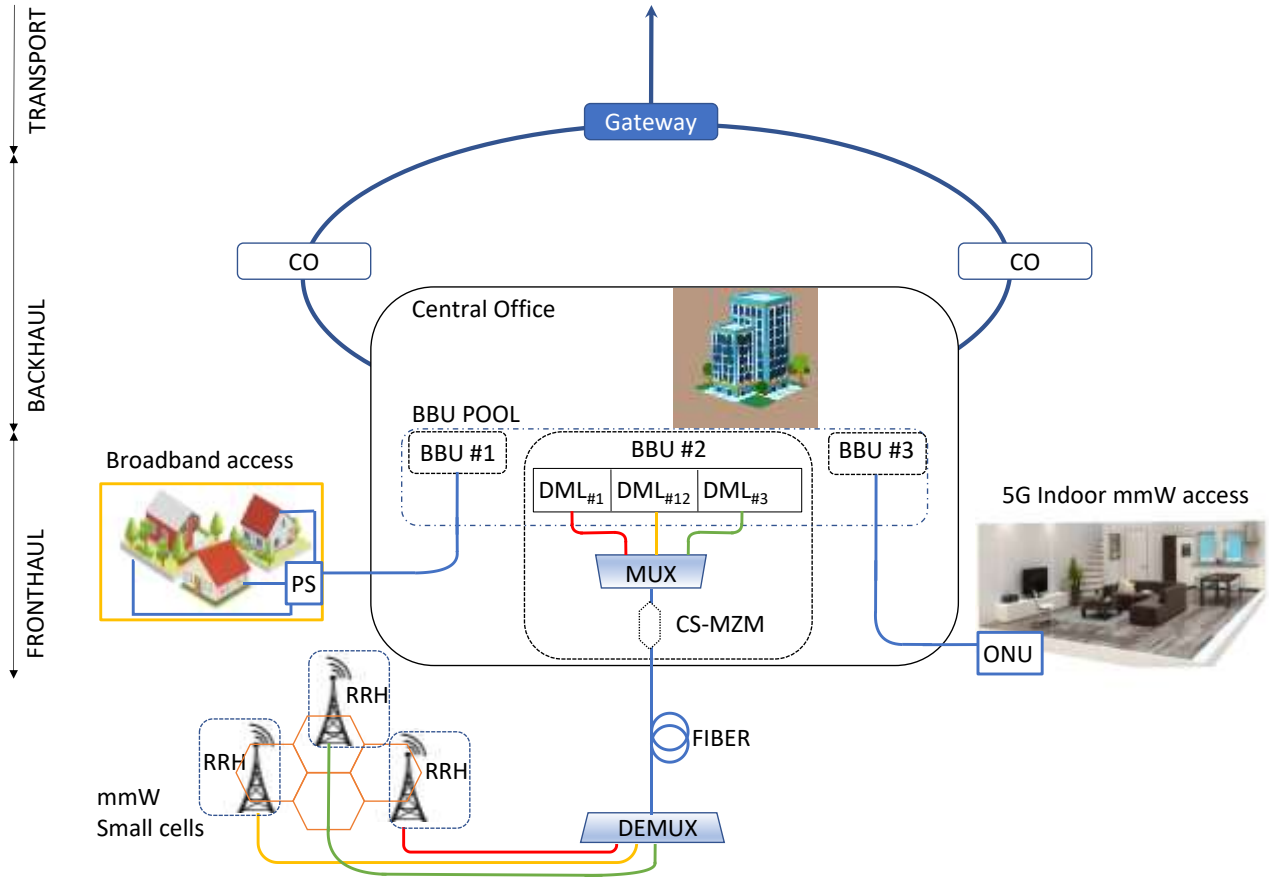

Fig. 1. 5G C-RAN architecture based on directly modulated lasers. CO: central office, PS: power splitter, BBU: baseband unit, DML: directly modulated laser, MUX: multiplexer, ONU: optical network user, CS-MZM: carrier suppressed-Mach Zehnder modulator, FSO: free space optics, RRH: radio remote head, mmW: millimetre wave.

optical fronthaul network connecting the RRHs with the centralized BBU pool. A backhaul segment is also defined between the BBUs and the gateway interface to the transport network. Therefore, RRHs are simplified since medium access control (MAC) layer functions, digital-to-analog and analog-to-digital conversion (DAC/ADC), radio frequency (RF) frontends and baseband processing are held in the BBUs located at the CO [17]. The BBU pool in this scenario includes an array of directly modulated lasers (DMLs) emitting at different wavelengths which are multiplexed for downlink transmission [18]. At the hotspot site, after channel demultiplexing, the optical receiver in each RRH performs the opto-electronic conversion and further amplification.

C-RAN also supports open platform and real-time virtualization technologies to provide dynamic shared resource allocation in the BBU pool, multi-vendor and native support to collaborative multipoint (CoMP) radio technologies due to the very low latency between BBUs hosted at the same pool. Broad coverage can be provided due to the large number of remote RRHs connected to a centralized BBU pool with a span fiber link, typically, up to 10 km for 5G or 20 km for 4G (LTE/LTE-A) [19].

A solution for the use of digital fiber optic interfaces in the 5G fronthaul network based on enhanced common public radio interface (eCPRI) has been recently proposed [20], although more complex RRHs and high bandwidth connections are required regardless the architectural choice for splitting the protocol functions [21, 22]. However, analog-radio-over-fiber (A-RoF) solutions are very promising for cost-efficient, low latency and large bandwidth links [23]. In the RoF scheme, mmW signals can be transmitted either using RF or an intermediate frequency (IF) over optical fiber. In the former one, the CO directly transmits the mmW signal, modulated into the optical domain, over fiber fronthaul network to the RRH without the need for frequency up-conversion at the RRH side. However, high speed photodetectors and optical transmitters are required and moreover, fiber chromatic dispersion has a significant impact on the link performance for high frequencies. On the contrary, the latter technique allows transportation of multiple aggregated IF bands modulated e.g. in low speed DMLs and the up-conversion is held at the RRH just before wireless transmission. The use of lower speed optoelectronic devices and reduced impact of fiber chromatic dispersion are the main advantages compared to a classic RoF approach, although the complexity and costs of RRHs are increased with the need for a mmW local oscillator and high speed mixers. However, mmW local oscillator delivery at the RRH has been demonstrated in the literature [24, 25] in order to provide flexibility in such systems and multiple IF bands employing OFDM formats have been transmitted up to several Gb/s bitrate [26].

As depicted in Fig. 1, in a centralized architecture, the

CS-MZM that provides photonic mmW signal generation is located at the BBU in the CO as part of the shared hardware infrastructure (i.e. remote generation scheme). However, a local generation scheme with the MZM located just before channel demultiplexing might be adopted to mitigate signal degradation for certain signals and network conditions since IF signal would be transmitted over fiber and the photonic up-conversion would be held before photodetection. The phase-noise of optically generated mmW signals based on external optical modulation techniques both locally and remotely has been previously studied in the literature [27]. In the former case, it is only determined by the phase noise of the electrical signal drive, whereas in the latter, its spectral quality is also affected by the chromatic dispersion of the fiber and the optical carrier linewidth. However, such degradation is negligible when the linewidth of the optical source is lower than 50 MHz and transmission distance is shorter than 50 km [27].

In this work, we evaluate the impact of the local and remote photonic generation of 40 GHz signal over an optical fronthaul based on a DML and CS external modulation for frequency up-conversion. For the first time to the authors´ knowledge, a full comprehensive study based on the analytical formulation to derive the frequency response of both approaches is provided, also supported by experimental measurements to identify the advantages and limitations of both setups. The results then can serve as a basis for future networks deployment based on photonic mmW signal generation.

The paper is structured as follows. Section II presents the analytical formulation of the local and remote approaches to obtain the system response at baseband and mmW band, which is confirmed by the experimental measurements over 25 km. Section III shows the system performance by transmitting a 250 MHz bandwidth QPSK signal centered at 0.5 GHz over 40 GHz measured at both bands under remote and local approaches in 10 and 25 km fiber links, also compared to back-to-back (B2B) links, then the characterization is completed with system measurements at several central frequencies for a 25 km fiber link. Finally, Section IV summarizes the main conclusions of this work.

II. Theoretical Background

Local and remote architectures for photonic mmW signal generation are evaluated in this section by obtaining the analytical expressions of the detected signals after photodetection. Fig. 2 shows a DML located at the BBU, which emits an optical carrier modulated by data in both schematics. On the one hand, in the local configuration depicted in Fig. 2 (a), the optical signal emitted by the DML is launched into the standard single mode fiber (SSMF) and then, it is up-converted by the f_{RF}=20 GHz single tone signal in the MZM, which is biased at null point for carrier suppressed modulation. However, in the remote configuration scheme depicted in Fig. 2(b), the DML output signal is launched into the CS-MZM to be modulated by an electrical single tone signal at f_{RF}=20 GHz and then, the resulting signal is transmitted through a SSMF link.

In the following, an analytical study of the frequency response of both approaches is presented for the sake of understanding and comparison, is also included the back-to-back performance as a reference.

The output electric field of a laser emitting at ω_0, which is directly modulated by a single tone at angular modulation frequency of $\Omega = 2\pi f$, can be described by [28]:

$$E_{DML}(t) = \sqrt{P_o(1 + m_{AM} \cdot cos\,\Omega t)}e^{jm_{PM}\cdot cos(\Omega t + \Delta\varphi)}e^{j\omega_0 t} \quad (1)$$

where P_o is the laser output power and m_{AM} and m_{PM} are the amplitude and phase modulation indexes, respectively. The phase difference between amplitude and phase modulation introduced by the laser is $\Delta\varphi$. It is possible to obtain the small-signal transfer function of the laser characterizing the chirp effect, which relates the amplitude and phase modulation terms to the linewidth enhacement factor, α, and adiabatic laser chirp, κ, as [28]:

$$\frac{m_{PM}}{m_{AM}} \cdot e^{j\Delta\varphi} = \alpha\left(1 - j\frac{\kappa P_o}{\Omega}\right) \quad (2)$$

In this small-signal regime, the intensity of electric field at the output of the light source can be defined as:

$$E_{DML}(t) = 1 + m_+ \cdot e^{j\Omega t} + m_- \cdot e^{-j\Omega t} \quad (3)$$

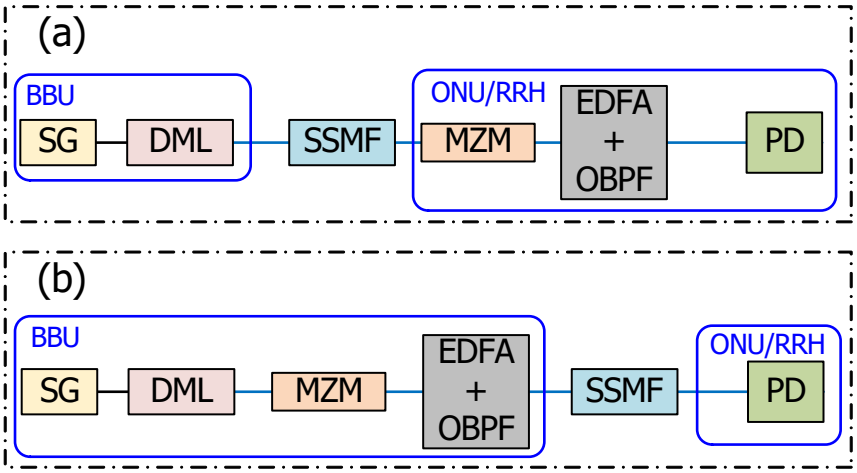

Fig. 2. Schematics for (a) local and (b) remote configuration. SG: signal generator, DML: directly modulated laser, MZM: Mach-Zehnder modulator, EDFA: erbium doped amplifier, OBPF: optical band pass filter, SSMF: standard single mode fiber, PD: photodetector.

where the index modulations, m_+ and m_-, are expressed in terms of amplitude, m_{AM}, and phase m_{PM} modulation index, as follows:

$$m_+ = \frac{1}{2}(m_{AM} + jm_{PM}e^{j\Delta\varphi})$$
$$m_- = \frac{1}{2}(m_{AM} + jm_{PM}e^{-j\Delta\varphi}) \quad (4)$$

Furthermore, let us consider the response of a MZM driven by a single tone at RF, $\Omega_{RF} = 2\pi f_{RF}$, given by:

$$h_{MZM}(t) = cos(\varphi_{DC} + 2m_{RF}\cos\Omega_{RF}t) \quad (5)$$

where φ_{DC} is the phase signal change caused by DC bias ($\varphi_{DC} = \pi/2$ in carrier suppression) and m_{RF} is the modulation RF index. Considering small-signal regime, we can obtain the following:

$$h_{MZM}(t) = cos\varphi_{DC} + m_{RF}sin\varphi_{DC} \cdot (e^{j\Omega_{RF}t} + e^{-j\Omega_{RF}t}) \quad (6)$$

The electrical current detected by the photodiode, $i(t)$, can be calculated as:

$$i(t) = \Re \cdot P(t) = \Re \cdot |E(t)|^2 \quad (7)$$

where $\Re$ is the photodiode responsivity, $P(t)$ is the detected optical power and $E(t)$ is the intensity of electric field at the input of the photodiode. Under small-signal assumption, the following expression can be calculated for optical back-to-back (OB2B) configuration from (3) and (5):

$$E_{B2B}(t) = E_{DML}(t) \cdot h_{MZM}(t) \quad (8)$$

Moreover, the impulse response of the signal propagation in SSMF fiber, $h_{SSMF}(t)$, can be expressed as [29]:

$$h_{SSMF}(t) = \frac{1}{\sqrt{j2\pi\beta_2 L}} e^{j\frac{\pi}{2\beta_2 L}t^2} \quad (9)$$

where L is the fiber length, and the dispersion parameter β_2 is the second derivative of the propagation constant with respect to the optical frequency ω_0.

According to the schematic depicted in Fig. 2(a) for the local configuration scheme, where the modulation process is held after the transmission of the DML output field over the dispersive element, the electric field at the input of the photodiode in this case, $E_{LC}(t)$, can be obtained from the following expression:

$$E_{LC}(t) = [E_{DML}(t) \otimes h_{SSMF}(t)] \cdot h_{MZM}(t) \quad (10)$$

Using (3), (6), (9) and (10), the electric field $E_{LC}(t)$ is obtained as:

$$\begin{aligned} E_{RC}(t) &= \sqrt{P_o}e^{j\omega_o t}\Big\{\cos\varphi_{DC} \\ &+ \cos\varphi_{DC}\, e^{j\frac{1}{2}\beta L\Omega^2}(m_+ \cdot e^{j\Omega t} + m_- \cdot e^{-j\Omega t}) \\ &+ m_{RF}\sin\varphi_{DC}\,(e^{j\Omega_{RF}t} + e^{-j\Omega_{RF}t}) \\ &+ m_{RF}\sin\varphi_{DC}\, e^{j\frac{1}{2}\beta L\Omega^2}\big(m_+ \cdot e^{j(\Omega_{RF}+\Omega)t} \\ &+ m_- \cdot e^{-j(\Omega_{RF}+\Omega)t}\big) \\ &+ m_{RF}\sin\varphi_{DC}\, e^{j\frac{1}{2}\beta L\Omega^2}\big(m_- \cdot e^{j(\Omega_{RF}-\Omega)t} \\ &+ m_+ \cdot e^{-j(\Omega_{RF}-\Omega)t}\big)\Big\} \end{aligned} \quad (11)$$

However, the remote configuration shown in Fig. 2(b) leads to a general expression for $E_{RC}(t)$ given by the convolution between the dispersive element and the electric field after modulation process:

$$E_{RC}(t) = [E_{DML}(t) \cdot h_{MZM}(t)] \otimes h_{SSMF}(t) \quad (12)$$

Concretely, the electric field for remote configuration $E_{RC}(t)$ can be obtained from (3), (6) and (9) by means of (12) as:

$$\begin{aligned} E_{RC}(t) = \sqrt{P_o}e^{j\omega_o t}\Big\{&\cos\varphi_{DC} \\ &+ \cos\varphi_{DC}\, e^{j\frac{1}{2}\beta L\Omega^2}(m_+ \cdot e^{j\Omega t} \\ &+ m_- \cdot e^{-j\Omega t}) \\ &+ m_{RF}\sin\varphi_{DC}\, e^{j\frac{1}{2}\beta L\Omega_{RF}^2}(e^{j\Omega_{RF}t} \\ &+ e^{-j\Omega_{RF}t}) \\ &+ m_{RF}\sin\varphi_{DC}\, e^{j\frac{1}{2}\beta L(\Omega_{RF}+\Omega)^2}\big(m_+ \\ &\cdot e^{j(\Omega_{RF}+\Omega)t} + m_- \cdot e^{-j(\Omega_{RF}+\Omega)t}\big) \\ &+ m_{RF}\sin\varphi_{DC}\, e^{j\frac{1}{2}\beta L(\Omega_{RF}-\Omega)^2}\big(m_- \\ &\cdot e^{j(\Omega_{RF}-\Omega)t} + \mathrm{m}_+ \cdot e^{-j(\Omega_{RF}-\Omega)t}\big)\Big\} \end{aligned} \quad (13)$$

In all cases, the calculation of the photocurrent $i(t)$ in (7) leads to different terms at baseband and mmW frequencies. For the sake of comparison, Table I shows the terms obtained for $i(t)$, which are proportional to the system transfer function under OB2B, local and remote configurations at Ω (baseband) and $2\Omega_{RF} \pm \Omega$ (mmW band), where the latter corresponds to the

TABLE I. ANALYTICAL TERMS OF THE PHOTOCURRENT $i(t)$ AT BASEBAND AND MMW BAND IN B2B, LOCAL AND REMOTE CONFIGURATIONS.

	CONFIG.	$i(t)$	
Ω	OB2B	$\Re P_o m_{AM} \cdot [cos^2\varphi_{DC} + 2m_{RF}^2 sin^2\varphi_{DC}]$	(14)
	LOCAL	$\Re P_o m_{AM}[cos^2\varphi_{DC} + 2m_{RF}^2 sin^2\varphi_{DC}] \cdot \left[\sqrt{1+\alpha^2}cos\left(\frac{1}{2}\beta_2 L\Omega^2 + atan\,\alpha\right) + j\alpha\frac{\kappa P_o}{\Omega}sin\left(\frac{1}{2}\beta_2 L\Omega^2\right)\right]$	(15)
	REMOTE	$\Re P_o\left[\sqrt{1+\alpha^2}cos\left(\frac{1}{2}\beta_2 L\Omega^2 + atan\,\alpha\right) + j\alpha\frac{\kappa P_o}{\Omega}sin\left(\frac{1}{2}\beta_2 L\Omega^2\right)\right] \cdot [m_{AM}cos^2\varphi_{DC} + 2m_{AM}m_{RF}^2 sin^2\varphi_{DC}cos(\beta_2 L\Omega_{RF}\Omega)]$	(16)
$2\Omega_{RF} \pm \Omega$	OB2B	$\Re P_o m_{AM} m_{RF}^2 sin^2\varphi_{DC}$	(17)
	LOCAL	$\Re P_o m_{AM} m_{RF}^2 sin^2\varphi_{DC} \cdot \left[\sqrt{1+\alpha^2}cos\left(\frac{1}{2}\beta_2 L\Omega^2 + atan\,\alpha\right) + j\alpha\frac{\kappa P_o}{\Omega}sin\left(\frac{1}{2}\beta_2 L\Omega^2\right)\right]$	(18)
	REMOTE	$\Re P_o m_{AM} m_{RF}^2 sin^2\varphi_{DC} \cdot \left[\sqrt{1+\alpha^2}cos\left(\frac{1}{2}\beta_2 L(\Omega^2 \pm 2\Omega_{RF}\Omega) + atan\alpha\right) + j\alpha\frac{\kappa P_o}{\Omega}\cdot sin\left(\frac{1}{2}\beta_2 L(\Omega^2 \pm 2\Omega_{RF}\Omega)\right)\right]$	(19)

TABLE II. THEORETICAL AND EXPERIMENTAL PARAMETERS.

	Parameter	Value
DML	λ	1553.45 nm
	P_o	4 mW
	α	1.5
	κ	14.9 GHz/mW
	m_{RF}	0.1
MZM	φ_{DC}	$\pi/2$
	m_{AM}	0.15
	f_{RF}	20 GHz
SSMF	β_2	$-22.1\,ps^2/km$
	L	25 Km

signal to be radiated by the base station.

Fig. 3 shows the theoretical system response and the corresponding electrical power measurement at baseband and mmW band respect to the carrier frequency of 40 GHz of the recovered signal after photodetection, where the parameters have been adjusted to those employed in the experimental setup, as detailed in Table II. Experimental measurements have been obtained employing a DML (Optical Zonu, OZ516) with a 3 dB bandwidth of 7.75 GHz and the system frequency response has been obtained using a signal generator (Rohde Schwarz, SMW200A) and a signal analyser (SA) (Rohde Schwarz, FSW43).

Experimental optical OB2B signals both at baseband and mmW band are shown in Fig. 3(a) and (b), respectively. Both transfer functions are proportional to the laser frequency response, which corresponds to the planar theoretical frequency response, as expected from (14) and (17) at baseband and mmW band, respectively.

Fig. 3(c) and (d) show the response for local configuration and, in this case, both bands show similar frequency dependence. Theoretical calculations using (15) and (18) lead to dispersion induced power fading for a laser directly modulated signal at frequencies given by:

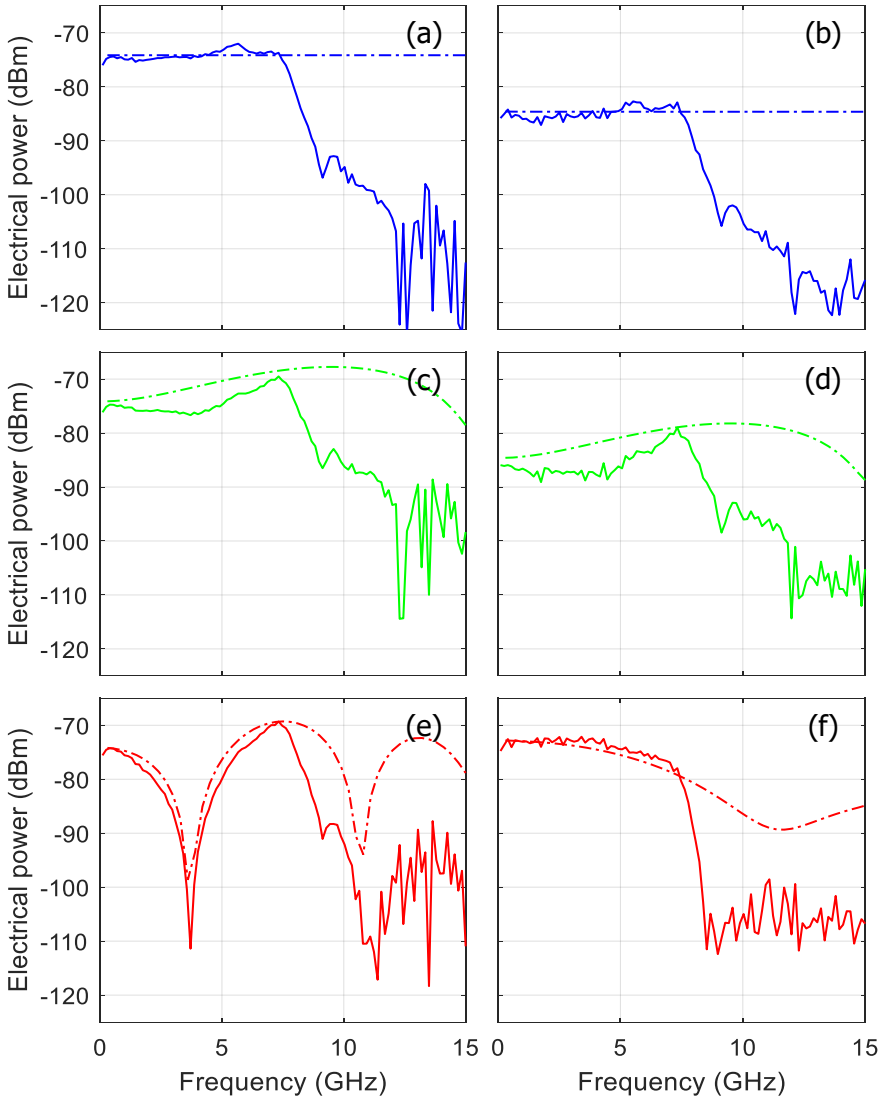

Fig. 3. Comparison of theoretical (dashed lines) and experimental (solid lines) electrical output power at baseband (left side) and mmW (right side) band: (a)-(b) OB2B, (c)-(d) local and (e)-(f) remote configurations, respectively. Both local and remote configurations are obtained over 25 km SSMF link.

$$\Omega_n \approx \sqrt{\left|\frac{(2n+1)\pi + 2\,atan\,\alpha}{\beta_2 L}\right|} \quad (n = 0,1,\dots) \qquad (20)$$

A 25 km fiber link leads to the first null ($n = 0$) at the frequency of 15.5 GHz, which is, however out of the laser operating bandwidth. Basically, the term related to phase contribution by means of κ is not significant in this RF frequency range. Experimental measurements at baseband and mmW band are limited by the laser modulation bandwidth and, therefore, show strong similarities to OB2B characterization.

However, the remote configuration leads to a system response, which is significantly different for both bands. According to (16), the first factor leads to the same nulls obtained in (20), which are out of the measuring frequency range. In this case, there are also nulls at frequencies causing the cancellation of the second factor in (16), which are given by:

$$\Omega_n = \frac{(2n+1)\pi}{2}\frac{1}{|\beta_2|L\Omega_{RF}} \quad (n = 0,1,\dots) \qquad (21)$$

The first null ($n = 0$) is obtained at 3.7 GHz for 25 km SSMF link, as shown in Fig. 3(e) both in the theoretical and experimental curves.

Oppositely, the remote configuration at mmW band (see (19)) only includes the term with nulls at frequencies given by (20), and therefore, no nulls are found within the laser bandwidth (see Fig. 3(f)). However, it is striking that the estimation of (19) at low frequencies, also confirmed by the experimental measurement, leads to a higher amplitude signal under the remote scheme compared to the local configuration as a result of the combined effect of dispersion and laser chirp,

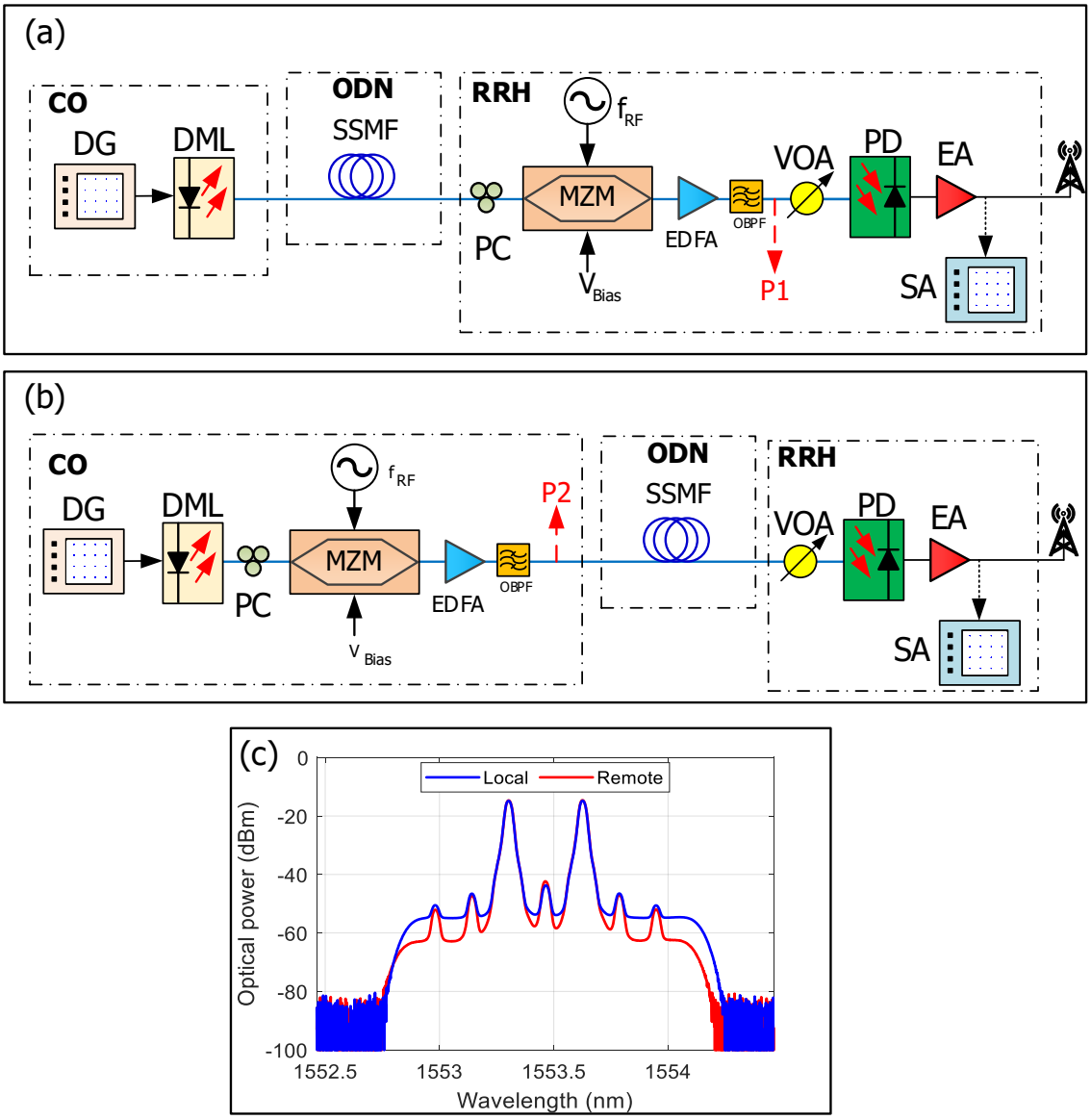

Fig. 4. Experimental setups for: (a) local microwave photonics (MWP) signal generation, (b) remote MWP signal generation and (c) optical spectrum of optically carrier suppressed modulated signal over 25 km SSMF at P1 in setup (a) –blue- and P2 in setup (b) –red-. CO: central office, DG: digital generator, DML: directly modulated laser, PC: polarization controller, MZM: Mach Zehnder modulator, EDFA: erbium doped amplifier, OBPF: optical band pass filter, ODN: optical distribution network, SSMF: standard single mode fiber, RRH: radio remote head, PD: photodetector, EA: electrical amplifier, SA: signal analyzer.

as has been previously observed [XX]. A signal gain of 15 dB with respect to local or OB2B configurations is measured for frequency values up to 8 GHz transmitted over 40 GHz. Note that this behaviour is not shown in baseband, as explained above.

III. Experimental Transmission Results

The experimental setups for local and remote mmW signal generation approaches are shown in Fig. 4. In this experiment, the same DML employed in the previous section emitting 5.6 dBm optical power was modulated by a 250 MHz bandwidth QPSK signal centered at 500 MHz, which was generated by the data generator (DG) (Rohde-Schwarz SMW200A) with a power of 5 dBm.

In the local generation scheme shown in Fig. 4(a), the directly modulated optical signal was transmitted along the SSMF fiber link, and just before PD conversion, it was up-converted by using a CS-MZM. The polarization of the optical signal was adjusted by a polarization controller (PC) and then this signal was launched into the MZM (Sumitomo T.DEH1.5-40X-ADC-Y-Z), which was biased at the null transmission point (V_π), i.e. 8.22 V, to obtain the carrier suppressed optical signal. The MZM was driven by a 20 GHz electrical single tone signal with 23 dBm electrical power, produced by a signal generator (Agilent 8267C). A fixed 17.5 dBm output power erbium doped fiber amplifier (EDFA) was set to compensate the optical losses, and the ASE noise was afterward filtered out by an optical band pass filter (OBPF) (Alnair BVF-100) with bandwidth $\Delta\lambda$=1.25 nm. Finally, the optoelectronic conversion was held into the photodetector (PD) (Finisar XPDV3120R) to generate an mmW signal at desired frequency by beating of sidebands.

As depicted in Fig. 4(b) corresponding to the remote scheme, after modulation in the CS-MZM, which was driven and biased in the same conditions as in the local scheme, the up-converted optical signal was transmitted over the SSMF link. Then, the

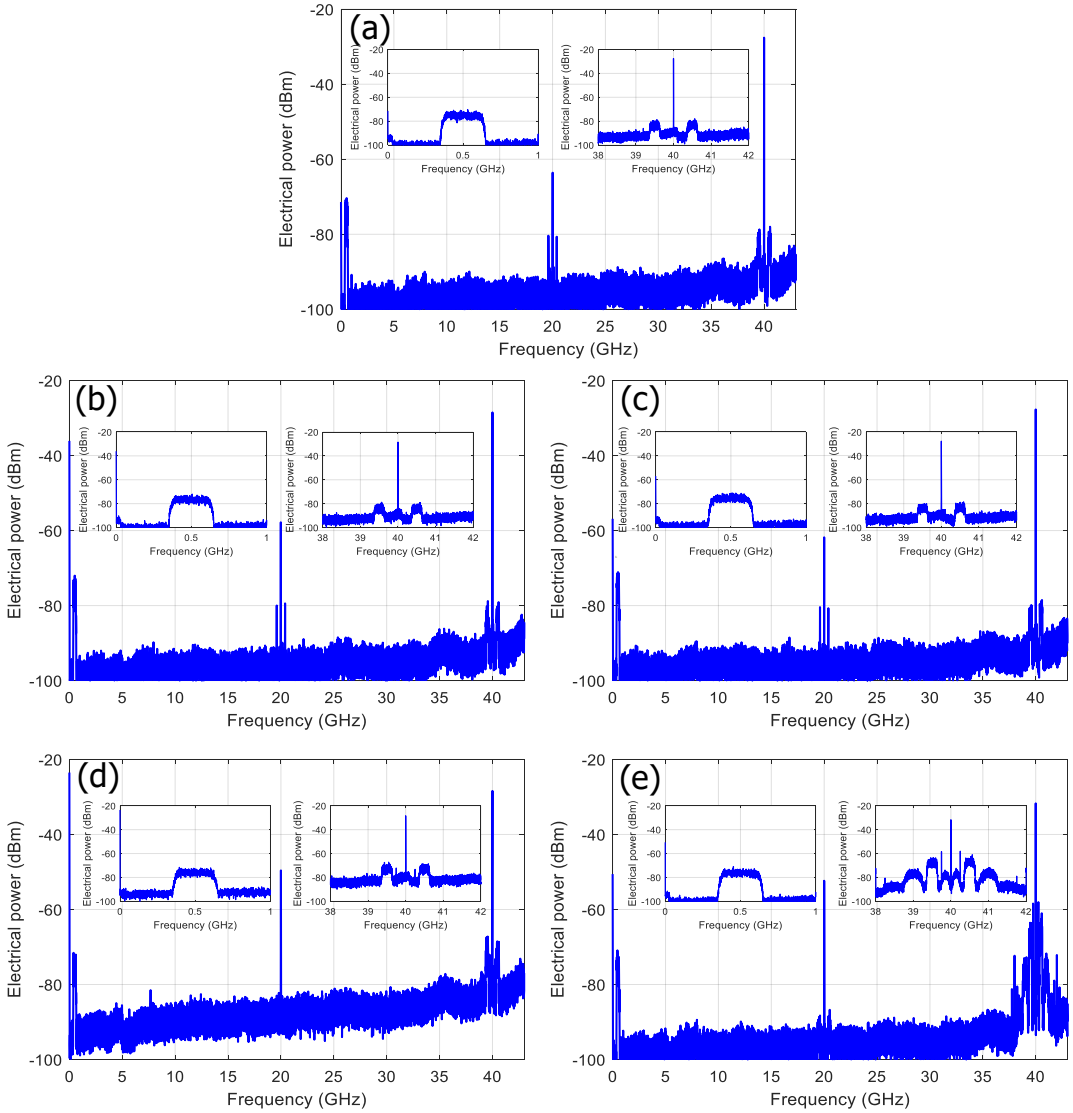

Fig. 5. Measured electrical spectra after photodetection with different configurations: (a) OB2B, (b) Local signal generation with 10km fiber link, (c) Local signal generation with 25 km fiber link, (d) Remote signal generation with 10 km fiber link, (e) Remote signal generation with 25 km fiber link; insets show the detail of the data band at baseband and at mmW band.

optical signal was amplified and filtered out by the EDFA and OBPF, respectively, and finally, the electrical signal was recovered at the 40 GHz band by the PD.

On the other hand, Fig. 5(d) and (e) show the measured electrical spectra for 10 and 25 km SSMF remote setup and no significant differences are found in data baseband with regards

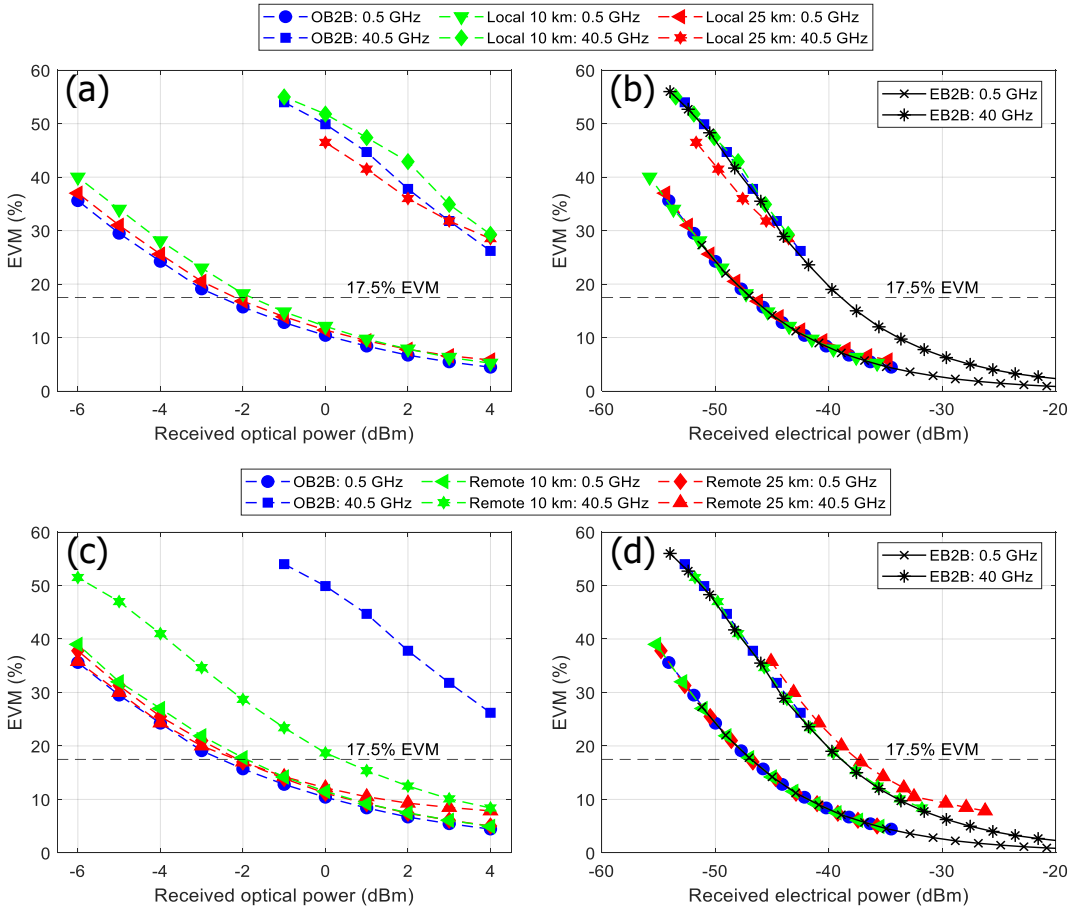

Fig. 6. EVM comparison at baseband and mmW bands between local and remote setups respect to B2B configuration for QPSK signal (IF=500 MHz) over 40 GHz for 10 and 25 SSMF links: (a) EVM vs RoP (local setup), (b) EVM vs electrical power (local setup), (c) EVM vs RoP (remote setup), (d) EVM vs electrical power (remote setup).

The optical spectrum at the OBPF output was measured at P1 and P2 points for local and remote schemes, as shown in Fig. 4(a) and Fig. 4(b), respectively, by an optical spectrum analyzer (OSA, Yokogawa AQ6370C), showing a carrier suppression larger than 26 dB (see Fig. 4(c)). It can be observed that ASE noise level is 10 dB lower in the remote setup due to higher gain saturation (higher optical power at the input of the EDFA).

The recovered electrical spectra after photodetection for OB2B, local and remote setups are depicted in Fig. 5. The mmW signal with -27.6 dBm electrical power is generated at 40 GHz, as shown by the electrical spectrum measured under OB2B setup in Fig. 5(a). The extinction ratio with respect to the original carrier at 20 GHz is higher than 36 dB and the insets show the detail of the data band at baseband (-75 dBm) and also at mmW band (-82 dBm).

Fig. 5(b) and (c) correspond to measurements under local configuration for 10 and 25 km SSMF, respectively, and lead to similar electrical power levels than OB2B both for baseband and mmW band, according to Fig. 3(c) and (d) (also in good agreement with (15) and (18)).

to OB2B. However, an electrical power increase of 9 and 16 dB is observed in data bands carried by mmW signal after transmission over 10 and 25 km fiber link, respectively. This fact confirms the results presented in previous section, where the electrical amplitude at the mmW band under remote configuration was found to be 15 dB larger with respect to OB2B ((19) and Fig. 3(f)) due to the system response. However, the remote configuration leads to high intermodulation (IMD) products at 40 GHz band in 25 km fiber link (see inset in Fig. 5(e)). Note that local configuration over the same link, shown in Fig. 5(e), does not exhibit IMD signals which can lead to dramatic penalties under certain signal conditions in remote generation setup, i.e. large bandwidth or multiband signals. Also, small residual bands appear around 20 GHz due to the lack of perfect carrier suppression in the MZM, which are more visible after the 25 km SSMF link.

In the following, the quality of the recovered signal after photodetection, i.e. the error vector magnitude (EVM), is measured by the SA, where 17.5% threshold level has been considered for QPSK modulation [30].

Fig. 6 shows the comparison between local (a)-(b) and

remote (c)-(d) setups transmission over 10 and 25 km of SSMF in terms of EVM performance at baseband (0.5 GHz) and also at mmW band (40.5 GHz) versus received optical power (RoP) and electrical power, respectively.

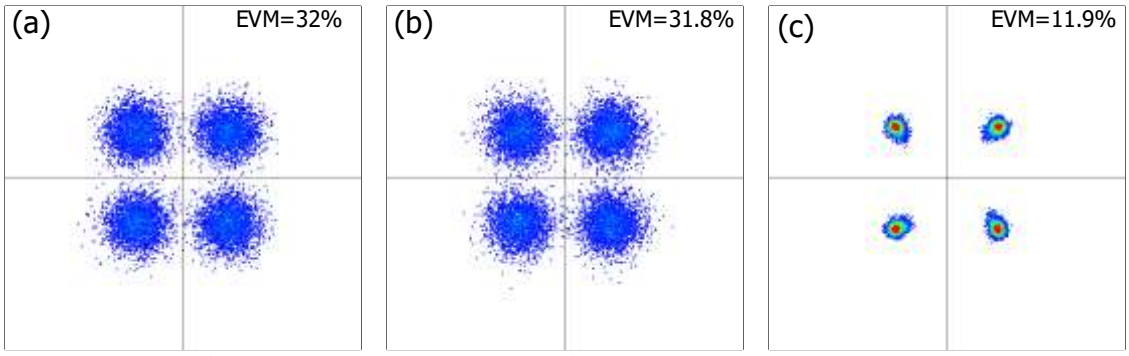

Fig. 7. Constellations at 3 dBm RoP for: (a) OB2B and over 25 km SSMF link for:(b) local and (c) remote setups.

As expected, local setup leads to signal transmission results over 10 and 25 km links with similar performance for a given RoP with respect to the OB2B, both at baseband and at mmW band as expected from the transfer functions in Fig. 3(c)-(d). Note that results obtained at 40.5 GHz show higher EVM due to bandwidth limitation of the laboratory equipment, as also shown in electrical B2B (EB2B) measurements. EVM measurements vs the received electrical power, shown in Fig. 6(b), confirm the quality of the signal strictly depends on the measured electrical power for both baseband and mmW band and no further penalties are present in the system as can be observed from the comparison with the EB2B measurements.

Additionally, Fig. 6(c) shows that EVM measurements over 10 and 25 km fiber transmission at baseband under remote setup, which are similar to those obtained in OB2B configuration, as expected from Fig. 3(e) at 0.5 GHz. Note that EVM values in OB2B at 40.5 GHz are significantly larger due to the equipment bandwidth limitations mentioned above. However, in this band, remote setup (Fig. 6(d)) leads to a significant signal quality improvement, i.e. EVM reduction, according to the frequency response depicted in Fig. 3(f) which leads to higher electrical power (i.e. 15 dB gain for 25 km) for fixed RoP. In our experiment, this improvement is estimated as an EVM decrease from 48% to 18.7 % and 12.2 % over 10 and 25 km, respectively, with 0 dBm RoP since electrical power increases with fiber length for fixed frequency and RoP. Moreover, Fig. 6(d) shows that EVM depends on the received electrical power for baseband and mmW band. In the mmW band, EVM OB2B measurements show 8 dB penalty with respect to baseband due to the bandwidth of the equipment but no further penalties are present and EVM keeps constant for a given electrical power level despite the fiber length.

Fig. 7 shows the measured constellations for OB2 over 25 km SSMF with 3 dBm RoP at 40.5 GHz. Spread symbols with EVM levels above the threshold are shown for OB2B (Fig. 7(a)) and local (Fig. 7(b)) configurations. Nevertheless, according to theoretical predictions explained above, a clearer constellation is recovered for remote configuration (Fig. 7(c)), where only aslight distortion is shown for the outer symbols due to the IMD.

The experimental work is completed by evaluating the system performance for different frequencies in order to confirm the theoretical and experimental frequency system response obtained in Section II of the paper. Fig. 8 shows EVM measurements and electrical received power as a function of the central frequency of the 250 MHz bandwidth QPSK signal both at baseband and at mmW band for OB2B, local and remote setups over 25 km fiber link.

Fig. 8(a) for OB2B shows a clear correlation between EVM and electrical power, as they result from the DML frequency response (see Fig. 3(a)). Electrical power decreases (i.e. EVM increases) due to the 7.75 GHz bandwidth limitation on the DML, so measurements are shown up to 8 GHz. Accordingly, measurements in the mmW band have been done from 32 GHz (8 GHz below the 40 GHz band) up to 43.5 GHz due to the SA bandwidth limitation. Again, the electrical power follows the predicted behaviour of the theoretical frequency response (see Fig. 3(b)) with corresponding EVM values where several EVM fluctuations are observed above the threshold.

Fig. 8(c) shows the electrical power and EVM measurement against frequency in baseband for local setup following the measured frequency response in Fig. 3(c), which is similar to that measured in OB2B setup. However, Fig. 8(d) shows some reduction (i.e. 2.5 dB at 35.5 GHz) of the electrical power with respect to the OB2B although a maximum is obtained at 7 GHz offset respect to 40 GHz, due to DML frequency response and also according to Fig. 3(d). Again, higher EVM values with some fluctuations due to signal processing are obtained above the threshold.

Finally, the performance of the remote generation setup is also characterized in frequency. Fig. 8(e) shows the electrical power decrease (i.e. EVM increase) at 3.7 GHz for remote setup, in good agreement with the notch predicted by (21) in baseband frequency response. However, Fig. 8(f) shows a 13 dB increase of electrical power (i.e. reduced EVM) with respect to OB2B along the measurement frequency range up to 35.5 GHz (4.5 GHz below 40 GHz) in accordance to Fig. 3(f).

IV. Conclusions

Remote and local photonic mmW signal generation setups have been compared in the deployment of a 5G C-RAN fronthaul

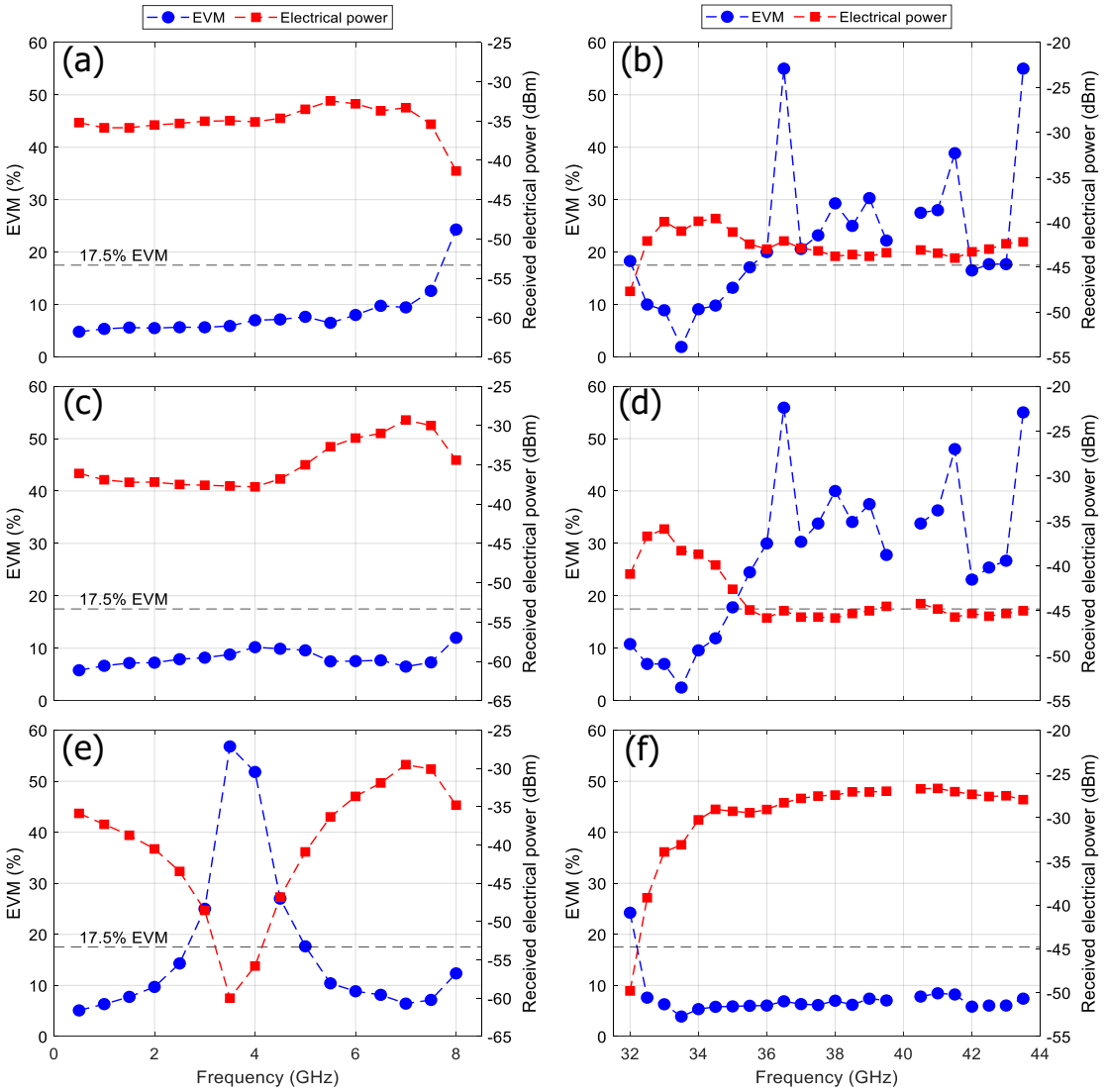

Fig. 8. EVM and received electrical power for different setups vs frequency over 25 km fiber link: (a)-(b) OB2B, (c)-(d) Local setup and (e)-(f) Remote setup, at baseband and millimeter wave band, respectively.

link in order to estimate the capabilities and limitations of both approaches. An optical fronthaul based on a DML and carrier suppressed external modulation for frequency multiplying has been considered and a full analytical formulation has been obtained to completely describe the baseband and mmW band terms of the system frequency response. Very good agreement has been shown between theory and measurements for both setups which leads to useful guidelines for future network design.

As expected, the local generation setup resembles the OB2B measurements both at baseband and mmW band since the dispersive effect at IF frequencies are less significant than RF frequencies. Accordingly, the remote scheme was expected to show worse performance since the dispersion is a non-negligible drawback for mmW transmitted signals. However, we have demonstrated that the remote setup leads to higher frequency response (i.e. 15 dB gain over 25 km fiber link) than the local setup in photonically generated mmW band due to the combined effect of dispersion and laser chirp, whereas the behaviour in baseband is significantly different.

Transmission experiments using a 250 MHz QPSK signal have been done for the sake of characterization of the system performance under remote and local generation setups measured at baseband and mmW band. As theoretically predicted, EVM experimental results in the remote generation scheme show better performance than OB2B, which is observed to increase with fiber length, whereas the local setup leads to similar performance than OB2B. Furthermore, EVM measurements under both setups lead to conclude that no further penalties are introduced by photonic mmW signal generation since EVM is mainly dependent on the electrical received power. Therefore, the amplitude response of the system presented in this paper provides the main guideline for photonically assisted mmW C-RAN network design. The measured electrical spectra show higher IMD products in remote generation schemes, which could cause significant penalties for specific scenarios, as will be evaluated in further work.

Finally, transmission experiments with data band at a different central frequency within the laser bandwidth have been also performed and again, full agreement has been obtained between theoretical and experimental results.

ACKNOWLEDGMENT

Generalitat Valenciana (PROMETEO 2017/103); Ministerio de Ciencia, Innovación y Universidades (FOCAL RTI2018-101658-B-I00); MEYES (LTC18008); Ministry of Industry and Trade in Czech Republic (FV40089) and within European Cooperation in Science and Technology (CA16220 and CA19111).

REFERENCES

[1] Cisco, “Cisco annual internet report (2018-2023),” White paper, 2020.
[2] Ericsson, “Ericsson mobility report,” 2020.
[3] ITU-R, “Report ITU-R M.2410-0. Minimum requirements related to technical performance for IMT-2020 radio interface(s),” 2017.
[4] C. Lim, Y. Tian, C. Ranaweera, T. A. Nirmalathas, E. Wong and K.-L. Lee, “Evolution of radio-over-fiber technology,” Journal of Lightwave Technology, vol. 37, no. 6, pp. 1647-1656, 2019.
[5] C. Ranaweera, E. Wong, A. Nirmalathas , C. Jayasundara and C. Lim, “5G C-RAN with optical fronthaul: an analysis from a deployment perspective,” Journal of Lightwave Technology, vol. 36, no. 11, pp. 2059-2068, 2018.
[6] I. Ajewale Alimi, A. L. Teixeira and P. Pereira Monteiro, “Toward an efficient C-RAN optical fronthaul for the future networks: a tutorial on technologies, requirements, challenges, and solutions,” IEEE Communications Surveys & Tutorials, vol. 20, no. 1, pp. 708-769, 2018.
[7] C. H. de Souza Lopes, E. Saia Lima, L. A. Melo Pereira, R. Maia Borges, A. Carvalho Ferreira, M. Abreu, W. Damascena Dias, D. H. Spadoti, L. Leonel Mendes and A. Cerqueira Sodre Junior, "Non-standalone 5G NR fiber-wireless system using FSO and fiber-optics fronthauls," Journal of Lightwave Technology, vol. 39, no. 2, pp. 406-417, 2021.
[8] H.-Y. Wang, Y.-C. Chi and G.-R. Lin, “Dual-mode laser diode carrier with orthogonal polarization and single-mode modulation for remote-node heterodyne MMW-RoF,” Optics Letters, vol. 41, no. 20, pp. 4676-4679, 2016.
[9] L. Gan, J. Liu, F. Li and P. K. A. Wai, “An optical millimeter-wave generator using optical higher order sideband injection locking in a Fabry–Pérot laser diode,” Journal of Lightwave Technology, vol. 33, no. 23, pp. 4985-4996, 2015.
[10] M. Hyodo, S. Saito and Y. Kasai, “Optical phase-locked loop with fibre lasers for low phase noise millimetre-wave signal generation,” Electronics Letters, vol. 45, no. 17, 2009.
[11] D. Novak, Z. Ahmed, R. B. Waterhouse and R. S. Tucker, “Signal generation using pulsed semiconductor lasers for application in millimeter-wave wireless links,” IEEE Transactions on Microwave Theory and Techniques, vol. 43, no. 9, pp. 2257-2262, 1995.
[12] P.-T. Shih, J. J. Chen, C.-T. Lin, W.-J. Jiang, H.-S. Huang and P.-C. Peng, “Optical millimeter-wave signal generation via frequency 12-tupling,” Journal of Lightwave Technology, vol. 28, no. 1, pp. 71-78, 2010.
[13] Y.-K. Seo, C.-S. Choi and W.-Y. Choi, “All-optical signal up-conversion for radio-on-fiber applications using cross-gain modulation in semiconductor optical amplifiers,” IEEE Photonics Technology Letters, vol. 14, no. 10, pp. 1448-1450, Oct. 2002.
[14] T. Schneider, M. Junker and D. Hannover, “Generation of millimetre-wave signals by stimulated Brillouin scattering for radio over fibre systems,” Electronics Letters, vol. 40, no. 23, pp. 295-304, 2004.
[15] S.-P. Dai, C.-T. Lin, S. Chi, P.-C. Peng and J. Chen, “Impact of nonlinear transfer function and imperfect splitting ratio of MZM on optical up-conversion employing double sideband with carrier suppression modulation,” Journal of Lightwave Technology, vol. 15, no. 2449-2459, p. 26, 2008.
[16] H. Zhang, L. Cai, S. Xie, K. Zhang, X. Wu and Z. Dong, “A novel radio-over-fiber system based on carrier suppressed frequency eightfold millimeter wave generation,” IEEE Photonics Journal, vol. 9, no. 5, 2017.
[17] C. Liu, J. Wang, L. Cheng, M. Zhu and G.-K. Chang, “Key microwave-photonics technologies for next-generation cloud-based radio access networks,” Journal of Lightwave Technology, vol. 20, no. 32, pp. 3452-3460, 2014.
[18] C.-T. Tsai, C.-H. Lin, C.-T. Lin, Y.-C. Chi and G.-R. Lin, “60-GHz Millimeter-wave Over Fiber with Directly Modulated Dual-mode Laser Diode,” Scientific Reports, vol. 6, no. 27919, 2016.
[19] J. Capmany and P. Muñoz, “Integrated microwave photonics for radio access netowrks,” Journal of Lightwave Technology, vol. 32, no. 16, pp. 2849-2861, 2014.
[20] C. P. R. Interface, “Common public radio interface: eCPRI interface specification,” 2019.
[21] E. Ruggeri, A. Tsakyridis, C. Vagionas, G. Kalfas, R. M. Oldenbeuving, P. W. L. Van Dijk, C. G. H. Roeloffzen, Y. Leiba, N. Pleros and A. Miliou, "A 5G fiber wireless 4Gb/s WDM fronthaul for flexible 360 coverage in V-Band massive MIMO small cells," Journal of Lightwave Technology, 2020.
[22] Intel, "Exploring 5G fronthaul network architecture intelligence splits and connectivity," White Paper, 2019.
[23] C. Mitsolidou, C. Vagionas, A. Mesodiakaki, P. Maniotis, G. Kalfas, C. G. H. Roeloffzen, P. W. L. van Dijk, R. M. Oldenbeuving, A. Miliou and N. Pleros, “A 5G C-ROptical fronthaul architecture for hotspot areas using OFDM-based analog IFoF waveforms,” Applied Sciences, vol. 9, no. 19, 2019.
[24] C. Lim, A. Nirmalathas, D. Novak, R. Waterhouse and G. Yoffe, “Millimeter-wave broad-band fiber-wireless system incorporating baseband data transmission over fiber and remote LO delivery,” Journal of Lightwave Technology, vol. 18, no. 10, pp. 1355-1363, 2000.
[25] T. Ismail, C. P. Liu and A. J. Seeds, “Millimetre-wave gigabit/s wireless-over-fibre transmission using low cost uncooled devices with remote local oscillator delivery,” OFC/NFOEC 2007 - 2007 Conference on Optical Fiber Communication and the National Fiber Optic Engineers Conference, 2007.
[26] N. Argyris, G. Giannoulis, K. Kanta, N. Iliadis, C. Vagionas, S. Papaioannou, G. Kalfas, D. Apostolopoulos, C. Caillaud, H. Debregeas, N. Pleros and H. Avramopoulos, “A 5G mmWave fiber-wireless IFoF analog mobile fronthaul link with up to 24-Gb/s multiband wireless capacity,” Journal of Lightwave Technology, vol. 37, no. 12, pp. 2883-2891, 2019.
[27] G. Qi, J. Yao, J. Seregelyi, S. Paquet, C. Belisle, X. Zhang, K. Wu and R. Kashyap, “Phase-noise analysis of optically generated millimeter-wave signals with external optical modulation techniques,” Journal of Lightwave Technology, vol. 24, no. 12, pp. 4861-4875, 2006.
[28] L. A. Neto, E. Didier, G. Naveena, C. Philippe, D. Qian, T. Fatoumata, A. Thomas, H. Rajaâ and A.-B. Christelle, “Simple estimation of fiber dispresion and laser chirp parameters using the downhill simplex fitting algorithm,” Journal of Lightwave Technology, vol. 31, no. 2, pp. 334 - 342, 13.
[29] I. P. Kaminow, T. Li and A. E. Willner, Optical Fiber Telecommunications Volume VIB: Systems and Networks, Academic Press, 2013.
[30] ETSI, “TS 138.101-2 V15.7.0. User Equipment (UE) radio transmission and reception; Part 2: Range 2 Standalone,” 2019.

Luis Vallejo was born in Malaga, Andalucia, Spain, in 1991. He received the B.Sc. degree in Telecommunication Technology Engineering in 2016 and the M.Sc in Telecommunication Engineering in 2017 from the Universidad de Malaga, Spain. He did a Test and Verification Engineer Internship at Keysight Technologies in 2017. He joined Instituto de Telecomunicaciones y Aplicaciones Multimedia (iTEAM), Photonic Research Labs (PRL), at the Universitat Politecnica de Valencia (UPV), Spain, in 2018. He is currently pursuing the PhD degree in Telecommunication Engineering program in UPV. His research interests include microwave photonics, mmW generation, RoF/FSO for 5G and beyond, and optical access networks.

José Mora was born in Torrent, Valencia, Spain, in 1976. He received the M.Sc. degree in Physical Sciences from the Universitat de València (Spain) in 1999. From 1999 to 2004, he worked in the Department on Applied Physics from the Universitat de València. He holds on a PhD. Degree in Physics from the Universitat de València in 2005 and he received the Extraordinary Doctorate Prize of the Universitat de València in 2006. Since 2004, he joined as a researcher at the Optical and Quantum Communications Group in the Institute of Telecomunications and Multimedia (ITEAM) from the Universitat Politècnica de València. He has been involved in the EU funded projects IST-LABELS, IST-GLAMOROUS, IST-OFFSOHO, IST-NEFERTITI and ICT-ALPHA. With an H-factor of 15, he has published more than 100 papers and conference contributions covering a wide range of fields related to fibre bragg gratings for sensing applications, optical signal processing, microwave photonics, reconfigurable and convergent optical for wired/wireless services and quantum cryptography using photonic technology.

Dong-Nhat Nguyen (S'15–M'19) received the B.Eng. (Hons) and Ph.D. degrees in electrical engineering from University of Nottingham, Malaysia Campus, Malaysia in 2014 and 2018, respectively. He is currently a postdoctoral researcher at Czech Technical University in Prague, Czech Republic. During spring 2017 and summer 2020, he was a visiting researcher at KAIST, Daejeon, South Korea and UPV, Valencia, Spain, respectively. His research interests include the seamless convergence of RF/Fiber/FSO for 5G and beyond, optical access networks, advanced modulation formats and signal processing.

Jan Bohata was born in Prague, Czech Republic, in 1988. He received the B.S. and M.S. degrees in communications, electronics, and multimedia from the Faculty of Electricalcv Engineering, Czech Technical University in Prague, in 2012, and the Ph.D. degree in radio electronics, in 2018. In 2012, he joined the Wireless and Fiber Optics Group, Department of Electromagnetic Field with a main focus on microwave photonics, fiber and free space optics networks, and optical communications in harsh environments. He is the author of more than 30 journal and conference papers and involved in a number of national and European research projects.

Vicenç Almenar was born in Valencia, Spain, in 1969. He received the Telecomunications Engineering and Ph.D. degrees from the Universitat Politècnica de València (UPV) in 1993 and 1999, respectively. In 2000, he did a Postdoctoral research stay at the Centre for Communications Systems Research (CCSR), University of Surrey, UK, where he was involved in research on digital signal processing for OFDM systems. He joined the Communications Department at UPV in 1993, became Associate Professor in 2002 and Professor in 2017; he was Deputy Director of the department from 2004 until 2014. His current research interests include OFDM, MIMO and signal processing techniques for wireless and optical communications systems.

Stanislav Zvanovec received the M.Sc. and Ph.D. degrees from the Faculty of Electrical Engineering, Czech Technical University (CTU) in Prague, in 2002 and 2006, respectively. He is currently works as a Full Professor, the Deputy Head of the Department of Electromagnetic Field, and the Chairperson of Ph.D. Branch with CTU. His current research interests include free space optical and fiber optical systems, visible light communications, OLED, RF over optics, and electromagnetic wave propagation issues for millimeter wave band. He is the author of two books (and coauthor of the recent book Visible Light Communications: Theory and Applications), several book chapters and more than 250 journal articles and conference papers.

Beatriz Ortega received the M.Sc. degree in Physics in 1995 from the Universidad de Valencia, and the Ph.D. in Telecommunications Engineering in 1999 from the Universidad Politécnica de Valencia. She currently works at the Departamento de Comunicaciones from the Universitat Politècnica de València, where she holds a Full Professorship since 2009 and collaborates as a group leader in the Photonics Research Labs in the Institute of Telecommunications and Multimedia Applications. She has published more than 200 papers and conference contributions in fibre Bragg gratings, microwave photonics and optical networks. She has got several patents and is also a co-founder of EPHOOX company. She has participated in a large number of European Networks of Excellence and R&D projects and other national ones. Her main research is currently focused on optical devices, optical networks and microwave photonic systems and applications